Inorg. Chem. **2006**, *45*, 8273–8282

Electronic Transitions in $[Re_6S_8X_6]^{4-}$ (X = Cl, Br, I): Results from Time-Dependent Density Functional Theory and Solid-State Calculations

Lindsay E. Roy and Timothy Hughbanks*

Department of Chemistry, Texas A&M University, P.O. Box 30012
College Station, Texas 77842-3012

Received June 13, 2006

Relativistic time-dependent density functional theory (TDDFT) calculations were performed on the excited states of the $[Re_6S_8X_6]^{4-}$ (X = Cl, Br, I) series. For all members of the series, the lowest excited states in the spectra do not correspond to a ligand-to-metal (or ligand-to-cluster) excitation but rather a cluster–cluster transition from the HOMO e_g to antibonding t_{1u} orbitals with only a modest admixture of Re–X σ^* character. These results lead to a re-evaluation of the role of the axial ligand in these compounds. The calculated excitation energies reproduce the experimental absorption and emission spectra. This work also confirms previous TDDFT calculations on the emission energies. Results for discrete cluster ions are compared with those obtained from calculations in the solid state in $Cs_4[Re_6S_8X_6]\cdot CsX$ (X = Cl, Br) and $Cs_4[Re_6S_8I_6]\cdot 2CsI$. Significant differences are seen in the relatively higher energies of the antibonding t_{1u} orbital in the solid-state case, and an inversion in the orbital character of the two allowed absorptions is calculated. The e_g (HOMO)-to-a_{2g} (LUMO) orbital energy differences corresponding to the emission transition are quite comparable for the solid state and discrete cluster calculations, and both overestimate the observed emission energy by the same margin.

Introduction

For more than two decades, the rich photophysical and photochemical properties of transition metal cluster compounds have sustained the interest of chemists and physicists who study them.[1,2] Related extended network compounds possessing polynuclear clusters as their principle structural feature are the superconducting Chevrel phases $PbMo_6Q_8$ (Q = S, Se, Te).[3–5] Discrete $M_6(\mu^3\text{-}Q)_8L_6$ include the intensely luminescent hexanuclear molybdenum(II) and tungsten(II) halide clusters $[M_6(\mu^3\text{-}X)_8X'_6]^{2-}$ (M = Mo, W; X, X′ = Cl, Br, I), which have been extensively studied.[6–17] The latter clusters are comprised of six metal atoms arranged in an octahedral core, with eight face-capping halides and six terminal donor ligands. These compounds display long-lived excited states and undergo facile ground- and excited-state multielectron transfer by electrogenerated chemiluminescence.[18–20] Such properties offer the potential for these clusters to play a central role in light-induced chemical reactions and optically based sensors.[21–24]

Rhenium analogues of the hexanuclear chalcogenide clusters, which are isostructural and isoelectronic with the

* To whom correspondence should be addressed. E-mail: trh@mail.chem.tamu.edu.

(1) Prokopuk, N.; Shriver, D. F. *Adv. Inorg. Chem.* **1998**, *46*, 1.
(2) Degroot, M. W.; Corrigan, J. F. *Comput. Coord. Chem. II* **2004**, *7*, 57.
(3) Srinivasan, R.; Sankaranarayanan, V. *Rev. Solid State Sci.* **1988**, *1*, 463.
(4) Chevrel, R.; Hirrien, M.; Sergent, M. *Polyhedron* **1986**, *5*, 87.
(5) Freeman, A. J.; Jarlborg, T. *Top. Curr. Phys.* **1982**, *34*, 167.
(6) Maverick, A. W.; Gray, H. B. *J. Am. Chem. Soc.* **1981**, *103*, 1298.
(7) Maverick, A. W.; Najdzionek, J. S.; MacKenzie, D.; Nocera, D. G.; Gray, H. B. *J. Am. Chem. Soc.* **1983**, *105*, 1878.
(8) Zietlow, T. C.; Schaefer, W. P.; Sadeghi, B.; Nocera, D. G.; Gray, H. B. *Inorg. Chem.* **1986**, *25*, 2198.
(9) Zietlow, T. C.; Nocera, D. G.; Gray, H. B. *Inorg. Chem.* **1986**, *25*, 1351.
(10) Nocera, D. G.; Gray, H. B. *J. Am. Chem. Soc.* **1984**, *106*, 824.
(11) Saito, Y.; Tanaka, H. K.; Sasaki, Y.; Azumi, T. *J. Phys. Chem.* **1985**, *89*, 4413.
(12) Cotton, F. A.; Stanley, G. G. *Chem. Phys. Lett.* **1978**, *58*, 450.
(13) Miki, H.; Ikeyama, T.; Sasaki, Y.; Azumi, T. *J. Phys. Chem.* **1992**, *96*, 3236.
(14) Preetz, W.; Harder, K.; Von Schnering, H. G.; Kliche, G.; Peters, K. *J. Alloys Compd.* **1992**, *183*, 413.
(15) Strauss, U.; Perchenek, N.; Ruehle, W. W.; Queisser, H. J.; Simon, A. *Chem. Phys. Lett.* **1993**, *202*, 415.
(16) Imoto, H.; Saito, T.; Adachi, H. *Inorg. Chem.* **1995**, *34*, 2415.
(17) Robinson, L. M.; Bain, R. L.; Shriver, D. F.; Ellis, D. E. *Inorg. Chem.* **1995**, *34*, 5588.
(18) Mussell, R. D.; Nocera, D. G. *J. Phys. Chem.* **1991**, *95*, 6919.
(19) Mussell, R. D.; Nocera, D. G. *Inorg. Chem.* **1990**, *29*, 3711.
(20) Mussell, R. D.; Nocera, D. G. *J. Am. Chem. Soc.* **1988**, *110*, 2764.
(21) Jackson, J. A.; Newsham, M. D.; Worsham, C.; Nocera, D. G. *Chem. Mater.* **1996**, *8*, 558.

10.1021/ic061061m CCC: $33.50
Published on Web 08/25/2006

molybdenum- and tungsten(II)-halide clusters, $[M_6(\mu^3\text{-}X)_8X'_6]^{2-}$, have been isolated as discrete species by dissolution of Re_6Q_8-containing solids in a process described as the "dimensional reduction" of the parent solid networks from which they originate.[25−27] For example, the addition of halide salts to melts of $Re_6S_8X_2$ (X = Cl, Br) affords cluster frameworks of reduced connectedness and dimensionality; two-dimensional sheets, one-dimensional chains, and discrete clusters.[25] Discrete $[Re_6S_8]^{2+}$ clusters exhibit red phosphorescence upon UV−visible excitation with emission lifetimes in the microsecond range.[27,28] In this respect, these clusters' properties are similar to those of the aforementioned molybdenum and tungsten halide clusters. The excitation has been classified by experimentalists as an axial-ligand-to-metal electron transfer, whereas the emission is thought to be axial-ligand independent.[25,28]

The promise of these clusters in various photochemical applications provides an incentive to establish the fundamental factors controlling their excited-state properties.[29−33] Despite the publication of several reports dealing with the electronic structure of these hexanuclear rhenium clusters, uncertainties remain concerning the nature of the electronic transitions and of their absorption and emission spectra. Early Dirac scattered-wave (SCF-DSW-Xα) calculations performed by Arratia-Pérez and Hernández-Acevedo yielded the assignments discussed above for the sulfido- and selenidorhenium clusters. These investigators were guided by similarities in results they obtained in calculations on the electronic structures for the luminescent $[W_6Cl_{14}]^{2-}$ cluster.[34,35] However, the transition energies, estimated as the energy difference between orbitals found near a halide-dominated HOMO and LUMO, were underestimated on the order of 0.8 eV in comparison with experimental results. Further calculations performed by Tanaka et al. examined the ground-state and a large number of excited-state wave functions using the ab initio configuration interaction (CI) method to elucidate the absorption and emission spectra.[36] Although the excitation energy was in good agreement with experimental peaks, the absorption spectra character was predicted as a mixture of metal-localized and ligand-to-metal charge-transfer transition. The emission transitions were also characterized as having a mixed metal-localized and a metal−ligand charge-transfer character. Later density functional theory (DFT) and Hartree−Fock (HF) calculations established that the HOMO is metal-based and that the emission can be described as a metal−metal transition, contradicting a previous Xα calculation, but description of the absorption excitations were not substantially changed.[27,35,37]

In connection with our long-standing interest in polynuclear metal clusters,[38−41] this paper seeks to extend the study of $[Re_6S_8]^{2+}$ clusters' electronic structure via time-dependent density functional theory (TDDFT) calculations. We will examine the influence that the high negative charge borne by these clusters has on their predicted optical properties by comparing calculations on clusters in vacuo and in the solid state. TDDFT provides a first-principles method for the calculation of excitation energies and oscillator strengths for which the reliability is now is well documented.[42−49] This method has been used with semiquantitative accuracy in many mononuclear complexes, but its use in polynuclear metal complexes has been limited.[50−58] Gray et al. used TDDFT computations in a study of the

(22) Jackson, J. A.; Mussell, R. D.; Nocera, D. G. *Inorg. Chem.* **1993**, *32*, 4643.
(23) Jackson, J. A.; Turro, C.; Newsham, M. D.; Nocera, D. G. *J. Phys. Chem.* **1990**, *94*, 4500.
(24) Ghosh, R. N.; Baker, G. L.; Ruud, C.; Nocera, D. G. *Appl. Phys. Lett.* **1999**, *75*, 2885.
(25) Long, J. R.; McCarty, L. S.; Holm, R. H. *J. Am. Chem. Soc.* **1996**, *118*, 4603.
(26) Long, J. R.; Williamson, A. S.; Holm, R. H. *Angew. Chem., Int. Ed. Engl.* **1995**, *34*, 226.
(27) Gray, T. G. *Coord. Chem. Rev.* **2003**, *243*, 213.
(28) Gray, T. G.; Rudzinski, C. M.; Meyer, E. E.; Holm, R. H.; Nocera, D. G. *J. Am. Chem. Soc.* **2003**, *125*, 4755.
(29) Tulsky, E. G.; Crawford, N. R. M.; Baudron, S. A.; Batail, P.; Long, J. R. *J. Am. Chem. Soc.* **2003**, *125*, 15543.
(30) Baudron, S. A.; Deluzet, A.; Boubekeur, K.; Batail, P. *Chem. Commun.* **2002**, 2124.
(31) Gabriel, J.-C. P.; Boubekeur, K.; Uriel, S.; Batail, P. *Chem. Rev.* **2001**, *101*, 2037.
(32) Gabriel, J. C.; Boubekeur, K.; Batail, P. *Inorg. Chem.* **1993**, *32*, 2894.
(33) For more information on electronic structure calculations of $[Re_6Q_8]^{2+}$ compounds: Yarovoi, S. S.; Mironov, Y. V.; Naumov, D. Y.; Gatilov, Y. V.; Kozlova, S. G.; Kim, S.-J.; Fedorov, V. E. *Eur. J. Inorg. Chem.* **2005**, 3945. Yarovoi, S. S.; Mironov, Y. V.; Solodovnikov, S. F.; Naumov, D. Y.; Moroz, N. K.; Kozlova, S. G.; Simon, A.; Fedorov, V. E. *Chem. Commun.* **2005**, 719. Baranovski, V. I.; Korolkov, D. V. *Polyhedron* **2004**, *23*, 1519. Baranovski, V. I.; Korolkov, D. V. *C. R. Chim.* **2005**, *8*, 1774. Tulsky, E. G.; Long, J. R. *Inorg. Chem.* **2001**, *40*, 6990. Tulsky, E. G.; Crawford, N. R. M.; Baudron, S. A.; Batail, P.; Long, J. R. *J. Am. Chem. Soc.* **2003**, *125*, 15543.
(34) Arratia-Perez, R.; Hernandez-Acevedo, L. *J. Chem. Phys.* **1999**, *111*, 168.
(35) Arratia-Perez, R.; Hernandez-Acevedo, L. *J. Chem. Phys.* **1999**, *110*, 2529.
(36) Honda, H.; Noro, T.; Tanaka, K.; Miyoshi, E. *J. Chem. Phys.* **2001**, *114*, 10791.
(37) Gray, T. G.; Rudzinski, C. M.; Meyer, E. E.; Nocera, D. G. *J. Phys. Chem. A* **2004**, *108*, 3238.
(38) Bond, M. R.; Hughbanks, T. *Inorg. Chem.* **1992**, *31*, 5015.
(39) Shen, J.; Hughbanks, T. *J. Phys. Chem. A* **2004**, *108*, 350.
(40) Magliocchi, C.; Xie, X.; Hughbanks, T. *Inorg. Chem.* **2004**, *43*, 1902.
(41) Xie, X.; Hughbanks, T. *Inorg. Chem.* **2002**, *41*, 1824.
(42) Van Gisbergen, S. J. A.; Guerra, C. F.; Baerends, E. J. *J. Comput. Chem.* **2000**, *21*, 1511.
(43) Te Velde, G.; Bickelhaupt, F. M.; Baerends, E. J.; Fonseca Guerra, C.; Van Gisbergen, S. J. A.; Snijders, J. G.; Ziegler, T. *J. Comput. Chem.* **2001**, *22*, 931.
(44) Marques, M. A. L.; Gross, E. K. U. *Lect. Notes Phys.* **2003**, *620*, 144.
(45) Burke, K.; Werschnik, J.; Gross, E. K. U. *J. Chem. Phys.* **2004**, 1.
(46) Van Gisbergen, S. J. A.; Baerends, E. J. *Comput. Coord. Chem. II* **2004**, *2*, 511.
(47) Wang, F.; Ziegler, T. *Mol. Phys.* **2004**, *102*, 2585.
(48) Marques, M. A. L.; Gross, E. K. U. *Proc. Int. Sch. Phys.* **2004**, *157*, 127.
(49) Marques, M. A. L.; Gross, E. K. U. *Annu. Rev. Phys. Chem.* **2004**, *55*, 427.
(50) Rosa, A.; Baerends, E. J.; van Gisbergen, S. J. A.; van Lenthe, E.; Groeneveld, J. A.; Snijders, J. G. *J. Am. Chem. Soc.* **1999**, *121*, 10356.
(51) Van Gisbergen, S. J. A.; Groeneveld, J. A.; Rosa, A.; Snijders, J. G.; Baerends, E. J. *J. Phys. Chem. A* **1999**, *103*, 6835.
(52) Ricciardi, G.; Rosa, A.; Baerends, E. J.; van Gisbergen, S. A. J. *J. Am. Chem. Soc.* **2002**, *124*, 12319.
(53) Ciofini, I.; Laine, P. P.; Bedioui, F.; Adamo, C. *J. Am. Chem. Soc.* **2004**, *126*, 10763.
(54) Batista, E. R.; Martin, R. L. *J. Phys. Chem. A* **2005**, *109*, 3128.
(55) Carrasco, R.; Cano, J.; Ottenwaelder, X.; Aukauloo, A.; Journaux, Y.; Ruiz-Garcia, R. *Dalton Trans.* **2005**, 2527.
(56) Clark, A. E.; Martin, R. L.; Hay, P. J.; Green, J. C.; Jantunen, K. C.; Kiplinger, J. L. *J. Phys. Chem. A* **2005**, *109*, 5481.
(57) Bollinger, J. C.; Chisholm, M. H.; Click, D. R.; Folting, K.; Hadad, C. M.; Tiedtke, D. B.; Wilson, P. J. *J. Chem. Soc., Dalton Trans.* **2001**, 2074.
(58) Wakamatsu, K.; Nishimoto, K.; Shibahara, T. *Inorg. Chem. Commun.* **2000**, *3*, 677.

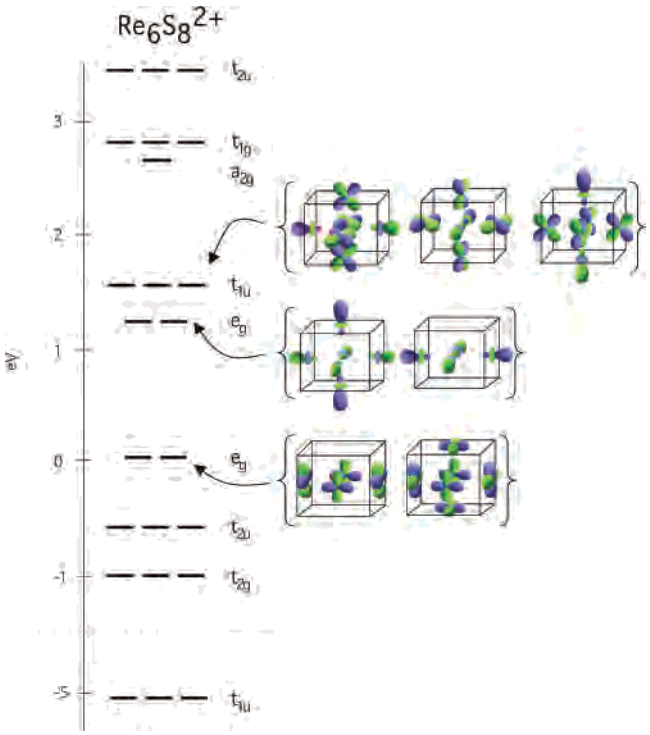

Figure 1. Re-based MOs for $[Re_6S_8]^{2+}$. Orbitals displayed have predominantly d_{z^2} or $d_{x^2-y^2}$ character.

effects that Jahn−Teller compression exerts upon the phosphorescence of $[Re_6S_8Cl_6]^{4-}$.[37] In addition, Kozlova used TDDFT calculations to analyze UV−vis spectra of $[Re_6Se_8(CN)_6]^{4-/3-}$ clusters.[59] However, these results do not fully explain the contributions to emission from four excited triplet-state sublevels.[60] We compare several functionals' abilities to reproduce both absorption and emission energies for $[Re_6S_8Cl_6]^{4-}$, and we re-examine the nature of their transitions.

While there are many calculations comparing the efficacy of different computational approaches, most such calculations are performed on ions in vacuo. We therefore conducted comparative calculations in which the generalized gradient BLYP functional was used both for calculations in vacuo and in the solid state. Specifically, we wanted to assess the relative importance of variations in computational methodology (e.g., variations in functionals) and the chemical/physical approximation made by use of isolated ions in calculations.

Computational Details

All calculations of geometry optimization and excitation properties of discrete model compounds were performed using density functional theory (DFT) in the Amsterdam density functional package (ADF).[43, 61]

The geometry optimization calculations were performed using either the local-density approximation characterized by the use of the homogeneous electron gas functional with the Vosko−Wilk−Nusair parametrization (VWN)[62] or one of the nonlocal exchange-correlation (xc) functionals described as follows. We used Becke nonlocal exchange[63] with either Perdew's nonlocal correlation functional[64] (BP86), or the Lee−Yang−Parr correlation functional[65] (BLYP). In all three cases, calculations were performed both nonrelativistically or within the scalar-relativistic zero order regular approximation (SR-ZORA).[66−68,69] We also carried out calculations using the meta-BLYP functional[70−76] with the SR-ZORA implementation. For relativistic calculations, we used the standard triple-ζ, double-polarization (TZ2P) Slater-type orbital (STO) basis functions for all atoms. The cores (Re, 1s−4d; S, 1s−2p; Cl, 1s−2p; Br, 1s−3p; I, 1s−4p) were treated within the frozen-core approximation. The Dirac utility was used to generate relativistic frozen core potentials for the SR-ZORA calculations. Nonrelativistic calculations employed the standard triple-ζ, single polarization (TZP) Slater-type orbital (STO) basis function for all atoms. The cores were kept frozen, as in the relativistic calculations. Spin−orbit zero order regular approximation calculations used all-electron TZ2P STO basis functions for all atoms and spin-restricted formalism. The integration parameter "accint" and the energy convergence criterion were set to 6 and 10^{-6} au, respectively. Symmetry was lifted in all ground-state geometry optimization calculations, and an open shell configuration was used except when indicated. Excited-state geometry optimizations of the clusters were performed under the constraints of the appropriate point group symmetry. All optimized geometries were verified by frequency calculations.

Excitation energies were obtained based on TDDFT, keeping the lowest 20 singlet and 20 triplet roots for vertical excitation from the ground state. In this work, we used the adiabatic local density approximation (ALDA) for the exchange-correlation kernel (in a post-SCF step).[77] It should be noted that spin−orbit coupling is not yet implemented for TDDFT in the ADF program. Symmetry

(59) Kozlova, S. G.; Gabuda, S. P.; Brylev, K. A.; Mironov, Y. V.; Fedorov, V. E. *J. Phys. Chem. A* **2004**, *108*, 10565.
(60) Kitamura, N.; Ueda, Y.; Ishizaka, S.; Yamada, K.; Aniya, M.; Sasaki, Y. *Inorg. Chem.* **2005**, *44*, 6308.
(61) Baerends, E. J.; Autschbach, J. A.; Bérces, A.; Bo, C.; Boerrigter, P. M.; Cavallo, L.; Chong, D. P.; Deng, L.; Dickson, R. M.; Ellis, D. E.; Fan, L.; Fischer, T. H.; Fonseca Guerra, C.; van Gisbergen, S. J. A.; Groeneveld, J. A.; Gritsenko, O. V.; Grüning, M.; Harris, F. E.; van den Hoek, P.; Jacobsen, H.; van Kessel, G.; Kootstra, F.; van Lenthe, E.; Osinga, V. P.; Patchkovskii, S.; Philipsen, P. H. T.; Post, D.; Pye, C. C.; Ravenek, W.; Ros, P.; Schipper, P. R. T.; Schreckenbach, G.; Snijders, J. G.; Sola, M.; Swart, M.; Swerhone, D.; te Velde, G.; Vernooijs, P.; Versluis, L.; Visser, O.; van Wezenbeek, E.; Wiesenekker, G.; Wolff, S. K.; Woo, T. K.; Ziegler, T. *ADF2004.01*, 2004.01; SCM, Theoretical Chemistry, Vrije Universiteit: Amsterdam, The Netherlands, 2004.
(62) Vosko, S. H.; Wilk, L.; Nusair, M. *Can. J. Phys.* **1980**, *58*, 1200.
(63) Becke, A. D. *Phys. Rev. A: At. Mol. Opt. Phys.* **1988**, *38*, 3098.
(64) Perdew, J. P. *Phys. Rev. B: Condens. Matter Mater. Res.* **1986**, *33*, 8822.
(65) Lee, C.; Yang, W.; Parr, R. G. *Phys. Rev. B: Condens. Matter Mater. Res.* **1988**, *37*, 785.
(66) van Lenthe, E.; Baerends, E. J.; Snijders, J. G. *J. Chem. Phys.* **1993**, *99*, 4597.
(67) van Lenthe, E.; Baerends, E. J.; Snijders, J. G. *J. Chem. Phys.* **1994**, *101*, 9783.
(68) Faas, S.; Snijders, J. G.; van Lenthe, J. H.; van Lenthe, E.; Baerends, E. J. *Chem. Phys. Lett.* **1995**, *246*, 632.
(69) van Lenthe, E.; Ehlers, A.; Baerends, E.-J. *J. Chem. Phys.* **1999**, *110*, 8943.
(70) Filatov, M.; Thiel, W. *Mol. Phys.* **1997**, *91*, 847.
(71) Sirois, S.; Proynov, E. I.; Nguyen, D. T.; Salahub, D. R. *J. Chem. Phys.* **1997**, *107*, 6770.
(72) Proynov, E. I.; Sirois, S.; Salahub, D. R. *Int. J. Quantum Chem.* **1997**, *64*, 427.
(73) Filatov, M.; Thiel, W. *Phys. Rev. A: At. Mol. Opt. Phys.* **1998**, *57*, 189.
(74) Van Voorhis, T.; Scuseria, G. E. *J. Chem. Phys.* **1998**, *109*, 400.
(75) Krieger, J. B.; Chen, J.; Iafrate, G. J.; Savin, A. *Electron Correl. Mater. Prop., Proc. Int. Workshop* **1999**, 463.
(76) Perdew, J. P.; Kurth, S.; Zupan, A.; Blaha, P. *Phys. Rev. Lett.* **1999**, *82*, 5179.
(77) Rosa, A.; Ricciardi, G.; Gritsenko, O.; Baerends, E. J. *Struct. Bonding* **2004**, *112*, 49.

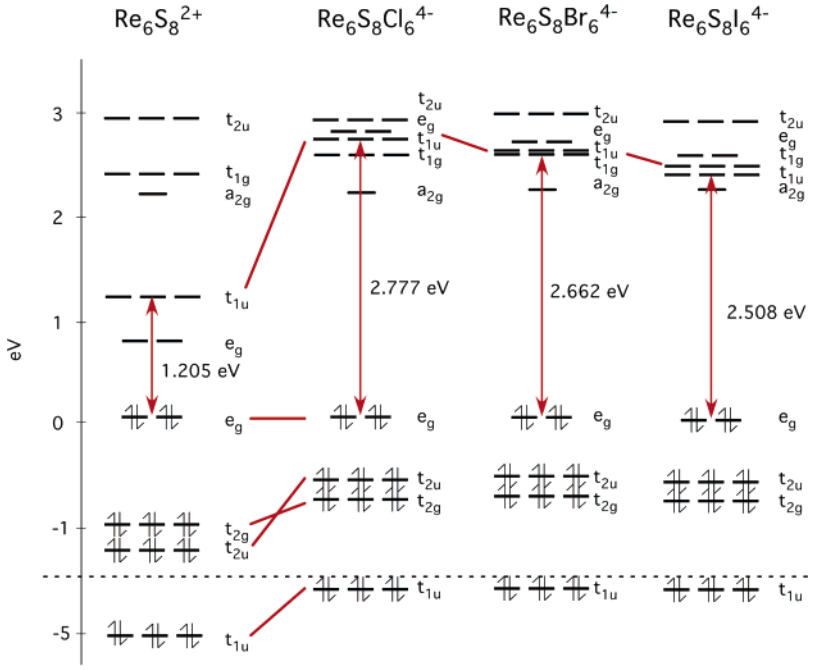

Figure 2. Changes in MO levels (LB94 functional) upon addition of halides to the $Re_6S_8^{2+}$ core.

for the ground-state cluster was set at O_h, and for the Franck−Condon singlet, D_{4h} (see Supporting Information). Typical approximate xc potentials do not have the correct asymptotic behavior for large inter-electronic distances, and excitation energies are consequently underestimated.[47] Therefore, we tested three different xc potentials; Becke−Lee−Yang−Parr (BLYP), the van Leeuwen−Baerends (LB94),[78] and the gradient-regulated asymptotic connection procedure applied to the BP potentials (BP-GRACLB).[79] The BLYP functional is a typical generalized gradient approximation (GGA) potential, and LB94 is an example of a so-called asymptotically correct potential. BP-GRACLB belongs to a class of shape-corrected potentials that also yield the correct asymptotic behavior. The BP-GRACLB potential sets the HOMO at the first ionization potential (IP) and therefore requires the IP as input. For this reason, the IP needed for the BP-GRACLB xc potential was taken from the BLYP gas-phase calculation and is in the Supporting Information.[80]

The electronic structure of the $[Re_6S_8X_6]^{4-}$ ion in the solid-state compounds $Cs_4[Re_6S_8Cl_6]\cdot CsCl$, $Cs_4[Re_6S_8Br_6]\cdot CsBr$, and $Cs_4[Re_6S_8I_6]\cdot 2CsI$ was also investigated by use of DFT based on structures determined by X-ray crystallography.[25] All solid-state calculations employed the BLYP functional from the DMol^3 program in the Cerius2 v4.9 suite of programs.[81−83] The double numerical basis function including d-polarization functions (DND) were employed in the calculation. Effective core potentials with frozen cores were used for the following elements (Re, 1s−4f; Br, 1s−3d; I, 1s−4f; Cs, 1s−4f). All calculations included scalar relativistic effects and open-shell configurations. The convergence criterion for the energy was set at 10^{-6} au and incorporated a fine integration grid. *P*1 symmetry was used in all calculations. Band calculations and quantities derived therefrom for $Cs_5[Re_6S_8X_6]X$ (X = Cl, Br) were carried out using a mesh of eight ***k***-points. In calculations on $Cs_6[Re_6S_8I_6]I_2$, eight ***k***-points were used. Orbital plots were obtained from ***k*** = 0 calculations. To calibrate these calculations in comparisons with those performed with the ADF package, we also performed gas-phase calculations on the $[Re_6S_8X_6]^{4-}$ ions using the DMol^3 program.

Results and Discussion

Electronic Structure of $[Re_6S_8X_6]^{4-}$. Before dealing with the excited states of the $[Re_6S_8X_6]^{4-}$ series, we will discuss the ground-state electronic structure of these molecules, with emphasis on differences due to halide variations. Trends in orbital energy gaps, which tend to correlate well with excitation energies, are of particular interest. The electronic structure of these "6−8 cluster types" has been the subject of many theoretical studies, but we will briefly review it here in order to place spectral trends in context.[84] Figure 1 shows a molecular orbital scheme for the $[Re_6S_8]^{2+}$ cluster; levels that have predominately Re 5d character are displayed. When referring to these clusters, we will adopt the convention that each metal atom has a local coordinate system such that each Re center's "z axis" is normal to the faces of the cube and the d_{xy} orbitals are directed toward the sulfur atoms. The highest occupied e_g orbital has local δ symmetry with respect to the *z* axes and therefore is little influenced by the terminal halides. The LUMOs are mainly radially directed e_g and t_{1u} orbitals, qualitatively characterized as having "z^2sp_z" hybrid character, and are the orbitals with which the rhenium atoms most strongly interact with the terminal halides. The bonding effects of the terminal halides can be viewed as a perturbation to the $[Re_6S_8]^{2+}$ electronic structure, as shown in Figure 2.[85]

To eliminate the orbital energy shift resulting from the overall charge, the relative orbital energies have been shifted

(78) van Leeuwen, R.; Baerends, E. J. *Phys. Rev. A: At. Mol. Opt. Phys.* **1994**, *49*, 2421.
(79) Gruning, M.; Gritsenko, O. V.; van Gisbergen, S. J. A.; Baerends, E. J. *J. Chem. Phys.* **2001**, *114*, 652.
(80) Jensen, L.; van Duijnen, P. T.; Snijders, J. G. *J. Chem. Phys.* **2003**, *119*, 12998.
(81) Delley, B. *J. Chem. Phys.* **2000**, *113*, 7756.
(82) Delley, B. *Comput. Mater. Sci.* **2000**, *17*, 122.
(83) Delley, B. *J. Chem. Phys.* **1990**, *92*, 508.
(84) Hughbanks, T.; Hoffmann, R. *J. Am. Chem. Soc.* **1983**, *105*, 1150.

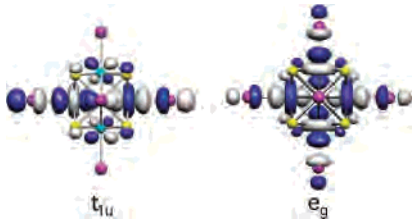

Figure 3. One each of the t_{1u} and e_g antibonding MOs.

in Figure 2 so that the e_g (HOMOs) are at the same level. Addition of the halides pushes up the a_{1g}, e_g, and t_{1u} orbitals with significant z^2 character, but the remaining orbitals are nearly unperturbed (relative to the e_g HOMO). The t_{1u}, t_{2g}, and t_{2u} orbitals are only weakly destabilized by the π-donation of the halide pπ orbitals. If the destabilizing effect on the e_g and t_{1u} orbitals is strong enough, the LUMO is the a_{2g} (modestly antibonding) molecular orbital. The latter orbital is solely metal-based, and presents a δ overlap to the terminal halides. Figure 3 depicts the plots of one of each of the antibonding t_{1u} and e_g orbitals. Upon moving from Cl to Br and I, there is a downward shift of Re−X antibonding orbitals (t_{1u} and e_g) because the Re/X overlap decreases as the size and diffuseness of the halide p orbitals increases. The t_{2u} orbitals remain nearly unchanged. The drop in energy of the e_g−t_{1u} orbitals is large enough that, in the case of X = I, these two orbital sets are below the a_{2g} orbital for all the functionals studied in this report, except LB94.

To summarize then, the $e_g(\sigma^*)$ and $t_{1u}(\sigma^*)$ orbital energies depend sensitively on the Re−X bond distances. Since orbital energy differences between occupied and virtual orbitals can be used as a first-order approximation of the excitation energies, this further underlines the sensitivity of our results to the Re−X distances used in excitation studies. We performed geometry optimization for the three members of the $[Re_6S_8X_6]^{4-}$ (X = Cl, Br, I) series using several functionals and compared results obtained with STO and Gaussian (GTO) basis sets, as well as results from relativistic and nonrelativistic GGA-DFT calculations.[28,86,87] The generalized gradient functionals (SR-ZORA) produce metal−metal bond lengths that are in good agreement with the experimental data, though distances that are systematically longer than those from experiment. Ironically, the structural optimizations conducted with the local density approximation (VWN) most closely match experiment, for these systems at least. The VWN method using SR-ZORA gives the most accurate bond lengths, with errors at 0.008 Å or less, but in some instances appears to slightly underestimate the bond length. This tendency of LDA to outperform GGA functionals is often seen in anionic complexes and has been explained as a fortuitous result of the overbinding tendencies of the LDA to compensate for the "Coulombic stress" suffered by gas-phase anionic systems.[88] Given our analysis of the optimized structures, we therefore conclude that the safest course in interpreting spectra is the use of experimental geometries. The current calculations take us a step further in spectral interpretation, since transition energies are explicitly computed and not merely estimated from orbital energy differences.

Electronic Spectra of $[Re_6S_8X_6]^{4-}$. Let us revisit the electronic spectrum of $[Re_6S_8X_6]^{4-}$ (X = Cl, Br, I) using the TDDFT method with adiabatic local density approximation. The excitation spectrum of $[Re_6S_8Cl_6]^{4-}$ exhibits a low-energy, low-intensity band (2.308 eV), and at higher energy, two more high-intensity peaks occur (2.856 and 3.289 eV).[25] The spectra of $[Re_6S_8Br_6]^{4-}$ and $[Re_6S_8I_6]^{4-}$ are very similar to the spectrum of $[Re_6S_8Cl_6]^{4-}$ and are dominated by two intense absorption bands.[25] However, one weak low-energy shoulder can be observed for the bromide analogue and is not observed in the iodide case. The clusters also emit red phosphorescence at low energy upon UV/visible excitation.[28,37,89] A definitive assignment of the excitation bands for either this cluster or the analogous molybdenum(II) and tungsten(II) $[M_6(\mu_3\text{-}X)_8X'_6]^{2-}$ (X, X′ = Cl, Br, I) cluster compounds has not been made. However, previous work suggests that the emission bands are attributed to transitions involving e_g HOMO and a_{2g} LUMO (using O_h symmetry).[7,27] The orbital energies from our calculations suggest that the e_g HOMO-to-a_{2g} LUMO excitations will yield the lowest excited states. Given this, we have described for the sake of our discussion the weak electronic absorption band as $^1E_g \leftarrow {}^1A_{1g}$ and the high-energy bands both as $^1T_{1u} \leftarrow {}^1A_{1g}$, the allowed transition. The $^1T_{1u} \leftarrow {}^1A_{1g}$ transition is the only one allowed by both spin and spatial symmetry. These transitions are depicted in Figure 4. We will also refer to the singlet−triplet calculations as an emission, but it should be clear that we calculated these transitions as an excitation. The calculated excitation and emission energies for the allowed and forbidden transitions for $[Re_6S_8X_6]^{4-}$ (X = Cl, Br, I) are presented in Table 1 and compared with the experimental information. The table also includes the composition of the excitation in terms of the major contributing one-electron transitions (contributions to solution vectors less than 1% are not reported).

An important conclusion to be drawn from the present TDDFT calculations is at variance with current experimental interpretations. The first allowed excitation is not well described as a "ligand-to-metal charge transfer" (nor ligand-to-cluster) as suggested by Long and co-workers.[25,28] Even in the absence of these calculations such a description seemed implausible; if the "originating orbital" in transition was primarily ligand-based, one would expect the magnitude of the red-shift upon moving through the series (Cl → I) would be much greater, as is observed in single metal atom complexes.[90,91] Our computational results indicate that the

(85) Note that the most prominent feature is the relative destabilization of the orbital energies for each hexanuclear rhenium cluster in the halide series. All orbital energies in the $[Re_6S_8X_6]^{4-}$ systems are strongly destabilized because of the anionic charge on these systems, but it is clear that the energy levels become more stabilized as one traverses the series (Cl → I). The orbital energy levels in the cationic $[Re_6S_8]^{2+}$ model lie much lower because of the positive charge.

(86) Deluzet, A.; Duclusaud, H.; Sautet, P.; Borshch, S. A. *Inorg. Chem.* **2002**, *41*, 2537.

(87) A full discussion and results can be found in the Supporting Information.

(88) Petrie, S.; Stranger, R. *Inorg. Chem.* **2004**, *43*, 2597.

(89) Gray, T. G.; Rudzinski, C. M.; Nocera, D. G.; Holm, R. H. *Inorg. Chem.* **1999**, *38*, 5932.

Table 1. TDDFT and Experimental Singlet−Singlet Excitation Energies (eV) for $[Re_6S_6X_6]^{4-}$ (X = Cl, Br, I)

	BLYP		LB94		BP-GRACLB		expt[25]
state	energy	composition	energy	composition	energy	composition	energy
				$[Re_6S_6Cl_6]^{4-}$			
$^1E_g \leftarrow {}^1A_{1g}$	2.901	86% ($1e_g \rightarrow 1a_{2g}$) 10% ($1e_g \rightarrow 2e_g$)	2.5101	93% ($1e_g \rightarrow 1a_{2g}$) 3% ($1e_g \rightarrow 2e_g$)	2.9547	80% ($1e_g \rightarrow 1a_{2g}$) 17% ($1e_g \rightarrow 2e_g$)	2.308
$^1T_{1u} \leftarrow {}^1A_{1g}$	2.9987	98% ($1e_g \rightarrow 1t_{1u}$)	2.8201	91% ($1e_g \rightarrow 1t_{1u}$) 7.5% ($1t_{2u} \rightarrow 1a_{2g}$)	3.0240	98% ($1e_g \rightarrow 1t_{1u}$)	2.857
$^1T_{1u} \leftarrow {}^1A_{1g}$	3.2833	73% ($1t_{2u} \rightarrow 1a_{2g}$) 26% ($1e_g \rightarrow 2t_{2u}$)	2.8880	79% ($1t_{2u} \rightarrow 1a_{2g}$) 13% ($1e_g \rightarrow 2t_{2u}$)	3.3354	75% ($1t_{2u} \rightarrow 1a_{2g}$) 24% ($1e_g \rightarrow 2t_{2u}$)	3.289
				$[Re_6S_6Br_6]^{4-}$			
$^1E_g \leftarrow {}^1A_{1g}$	2.8782	61% ($1e_g \rightarrow 2e_g$) 38% ($1e_g \rightarrow 1a_{2g}$)	2.5402	89% ($1e_g \rightarrow 1a_{2g}$) 6% ($1e_g \rightarrow 2e_g$)	2.9013	77% ($1e_g \rightarrow 2e_g$) 22% ($1e_g \rightarrow 1a_{2g}$)	2.275
$^1T_{1u} \leftarrow {}^1A_{1g}$	2.8152	99% ($1e_g \rightarrow 1t_{1u}$)	2.7124	96% ($1e_g \rightarrow 1t_{1u}$) 2% ($1t_{2u} \rightarrow 1a_{2g}$)	2.8364	99% ($1e_g \rightarrow 1t_{1u}$)	2.798
$^1T_{1u} \leftarrow {}^1A_{1g}$	3.3080	77% ($1t_{2u} \rightarrow 1a_{2g}$) 22% ($1e_g \rightarrow 2t_{2u}$)	2.8481	90% ($1t_{2u} \rightarrow 1a_{2g}$) 7% ($1e_g \rightarrow 2t_{2u}$)	3.3641	79% ($1t_{2u} \rightarrow 1a_{2g}$) 20% ($1e_g \rightarrow 2t_{2u}$)	3.092
				$[Re_6S_6I_6]^{4-}$			
$^1T_{1u} \leftarrow {}^1A_{1g}$	2.5525	99% ($1e_g \rightarrow 1t_{1u}$)	2.5436	96% ($1e_g \rightarrow 1t_{1u}$) 2% ($1t_{2u} \rightarrow 1a_{2g}$)	2.5438	99% ($1e_g \rightarrow 1t_{1u}$)	2.445
$^1T_{1u} \leftarrow {}^1A_{1g}$	3.2324	83% ($1t_{2u} \rightarrow 1a_{2g}$) 14% ($1e_g \rightarrow 2t_{2u}$)	2.6537	94% ($1t_{2u} \rightarrow 1a_{2g}$) 2% ($1e_g \rightarrow 2t_{2u}$)	3.2883	83% ($1t_{2u} \rightarrow 1a_{2g}$) 13% ($1e_g \rightarrow 2t_{2u}$)	2.952

lowest excited states involve metal-based orbitals for all the functionals studied. The orbitally forbidden $^1E_g \leftarrow {}^1A_{1g}$ excitation is the lowest in energy and involves cluster bonding−antibonding transitions. The composition of the two allowed $^1T_{1u} \leftarrow {}^1A_{1g}$ states varies a little from one functional to another. In all functionals, the lower-energy transition involves primarily a $1e_g \rightarrow 1t_{1u}$ (see Figure 4) orbital excitation (>90%) and the latter transition has more mixed parentage involving cluster−ligand pπ-to-metal−metal antibonding excitation ($1t_{2u} \rightarrow 1a_{2g}$ and $1e_g \rightarrow 2t_{2u}$), which is still best described as a cluster bonding−antibonding transition. The only occupied orbitals near the frontier orbitals that are solely "ligand based" reside ~0.6 eV below the HOMO and contribute <0.06% and <0.03% to the two lowest allowed excitations, respectively. The Re−Re and Re−S bonds are nearly unaltered upon halide exchange, and the energy of the weak absorption remains nearly constant even as the terminal ligand changes (the lowest absorption energy for $[Re_6S_8Cl_6]^{4-}$ and $[Re_6S_8Br_6]^{4-}$ is 2.308 and 2.275 eV, respectively). Presumably then, the first allowed excitation in the $[Re_6S_8I_6]^{4-}$ cluster obscures the weak forbidden absorption peak.

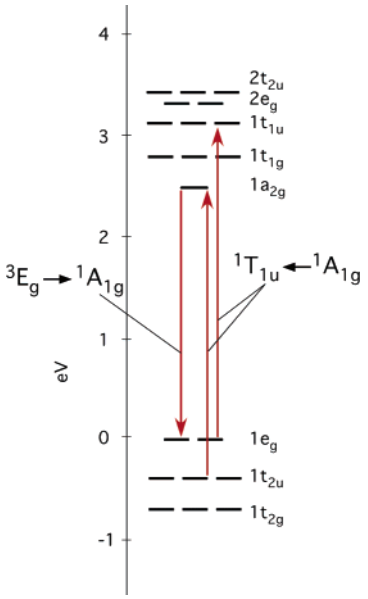

Figure 4. Energy-level scheme outlining the observed transitions.

In the singlet excited-state manifold for $[Re_6S_8X_6]^{4-}$ (X = Br, I), the lowest excited state is now predicted to be the first allowed $^1T_{1u} \leftarrow {}^1A_{1g}$ excitation, which is consistent with the downward shift in energy of both the radially directed e_g/t_{1u} orbitals upon halide exchange from Cl to Br and I that occurs in the gas phase. The weak absorption, which was the lowest-energy transition in the $[Re_6S_8Cl_6]^{4-}$ case, is now only predicted to be the lowest-energy transition when using the LB94 functional.

The agreement with the first experimental band for $[Re_6S_8I_6]^{4-}$ is satisfactory, but all functionals predict the energy too high. One point touched upon earlier was the ordering of the a_{2g} LUMO and the e_g/t_{1u} unoccupied orbitals for the iodide cluster. For this transition, BLYP and BP-GRACLB calculations indicate that the radially directed orbitals lie lower than the a_{2g} LUMO counterpart of the $[Re_6S_8X_6]^{4-}$ cluster, but not in the case of the LB94 functional. These irregularities may stem from the functionals' inadequacies concerning the strength of the metal−iodide bond.

Spin−orbit coupling will have some effect on the excitation energies for $[Re_6S_8X_6]^{4-}$ (X = Cl, Br, I) and in particular the iodide analogue, but we were unable to further investigate this aspect because spin−orbit effects are not yet available for TDDFT. However, the magnitude of the spin−orbit effects is expected to be small. A first-order approximation can be obtained from the orbital energies that implement spin−orbit effects. When spin−orbit coupling is included in the SCF calculation, the e_g HOMO−t_{1u} orbital energy difference decreased by ~0.3 eV for the clusters (see Table 4). There is, of course, a large energy difference at the *scalar* relativistic level (on the order of 2.5 eV).

(90) Buhr, J. D.; Winkler, J. R.; Taube, H. *Inorg. Chem.* **1980**, *19*, 2416.
(91) Isci, H.; Mason, W. R. *Inorg. Chem.* **1983**, *22*, 2266.

Table 2. TDDFT Triplet−Singlet Emission Energies (eV) $[Re_6S_6X_6]^{4-}$ (X = Cl, Br, I)

	BLYP		LB94		BP-GRACLB		expt[28 a]
state	energy	composition	energy	composition	energy	composition	energy
			$[Re_6S_6Cl_6]^{4-}$				
$^3B_{1g} \rightarrow {}^1A_{1g}$ (D_{4h}^{comp})	2.2009	98% ($1a_{1g} \rightarrow 2b_{1g}$)	1.8068	98% ($1a_{1g} \rightarrow 2b_{1g}$)	2.2623	98% ($1a_{1g} \rightarrow 2b_{1g}$)	1.475
$^3A_{1g} \rightarrow {}^1A_{1g}$ (D_{4h}^{el})	2.1910	97% ($1b_{1g} \rightarrow 2b_{1g}$)	1.7984	96% ($1b_{1g} \rightarrow 2b_{1g}$)	2.2523	94% ($1b_{1g} \rightarrow 2b_{1g}$)	
			$[Re_6S_6Br_6]^{4-}$				
$^3B_{1g} \rightarrow {}^1A_{1g}$ (D_{4h}^{comp})	2.1893	97% ($1a_{1g} \rightarrow 2b_{1g}$)	1.8014	98% ($1a_{1g} \rightarrow 2b_{1g}$)	2.2492	96% ($1a_{1g} \rightarrow 2b_{1g}$)	1.442
			$[Re_6S_6I_6]^{4-}$				
$^3B_{1g} \rightarrow {}^1A_{1g}$ (D_{4h}^{comp})	2.1551	96% ($1a_{1g} \rightarrow 2b_{1g}$)	1.7830	97% ($1a_{1g} \rightarrow 2b_{1g}$)	2.2109	71% ($1a_{1g} \rightarrow 2b_{1g}$) 26% ($1a_{1g} \rightarrow 3b_{1g}$)[b]	1.364

[a] Solid-state emission energy at 75 K. [b] $3b_{1g}$ is from the splitting of the e_g Re−X σ^*.

Nocera and co-workers predicted that, upon excitation, the cluster undergoes a tetragonal compression as a result of the partially filled e_g HOMO in O_h symmetry.[37] Upon tetragonal compression, the e_g (O_h) orbital set splits such that the a_{1g} (D_{4h}) becomes a SOMO (singly occupied MO) and the b_{1g} (D_{4h}) orbital is fully occupied. The higher-lying a_{2g} orbital in O_h symmetry becomes b_{1g} in D_{4h} symmetry and is singly occupied, as illustrated in Chart 1. The $b_{1g}{}^2a_{1g}{}^1b_{1g}{}^1$ configuration yields long Re−Re basal bonds and only a slight lengthening of the Re_{apical}−Re_{basal} distance compared to the ground state. Because of symmetry lowering, the spin- and orbitally forbidden lowest emission becomes a $^3B_{1g} \rightarrow {}^1A_{1g}$ transition, corresponding to the HOMO−LUMO orbitals a_{1g} and b_{1g} (D_{4h}).

Chart 1

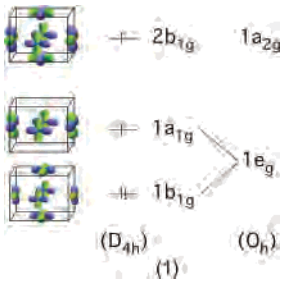

TDDFT yields energies for the singlet−triplet transitions for $[Re_6S_8X_6]^{4-}$ (X = Cl, Br, I) of the D_{4h}-compressed "Franck−Condon singlet" that are ∼0.3 eV larger than experimentally observed (Table 2).[92−94] These results confirm previous studies' TDDFT results on $[Re_6S_8Cl_6]^{4-}$ by Nocera and co-workers who used an admixture of 24.3% Hartree−Fock exchange to the BP86 functional to achieve an exact emission energy for the $^3B_{1g} \rightarrow {}^1A_{1g}$ transition compared to experiment.[27] However, Kitamura and co-workers found that the emission spectra can be explained by four lowest-energy excited triplet state sublevels.[60] We find it unlikely that the emitting states can be accounted for solely by invoking the tetragonally elongated structure, mentioned in the Supporting Information, to be only 50 cm^{-1} higher in energy compared to the compressed D_{4h} geometry. Aside from an expected thermal expansion, the clusters do not alter their ground-state structure with temperature.[30] Spin−orbit coupling is likely to be substantial for these rhenium-based systems and will split both lower and upper excited states ($^3B_{1g}$, derived from the $b_{1g}{}^2a_{1g}{}^1b_{1g}{}^1$ (D_{4h}) compressed configuration; $^3A_{1g}$, derived from the $b_{1g}{}^1a_{1g}{}^2b_{1g}{}^1$ (D_{4h}) elongated configuration) and will mix a doubly degenerate spin−orbit state from each together. Comparison of emission lifetimes for the $[Re_6S_8X_6]^{4-}$ and $[M_6X_{14}]^{2-}$ (M = Mo, W; X = Cl, Br) bolsters this analysis: the greater spin−orbit coupling extant for W and Re should produce shorter lifetimes.[7,28,95]

To summarize, gas-phase calculations predict that the low-energy spin- and orbitally allowed transitions are cluster bonding−antibonding excitations from the HOMO e_g set to the t_{1u} unoccupied orbitals. Calculations reveal that the LB94 functional most closely predicts the excitation energy of the first $^1T_{1u} \leftarrow {}^1A_{1g}$ transition, but it yields results too low for

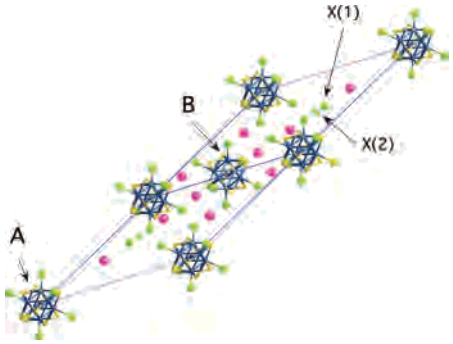

Figure 5. $Cs_4[Re_6S_8X_6]\cdot CsX$ (X = Cl, Br) shown in the rhombohedral setting. Clusters at (0,0,0) and ($^1/_2$, $^1/_2$, $^1/_2$) are, respectively, labeled as **A** and **B**. The half-occupied X(1) and X(2) positions, the former was filled and the latter vacant.

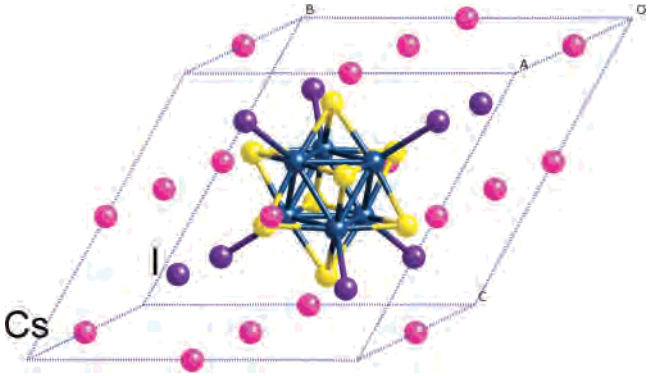

Figure 6. $Cs_4[Re_6S_8I_6]\cdot 2CsI$ shown in the primitive setting.

(92) The term "Franck−Condon singlet" refers to the ground-state cluster in D_{4h}-triplet geometry.
(93) For a full discussion of our geometry-optimization calculations of the Jahn−Teller distorted structure, please refer to the Supporting Information.
(94) We experienced no difficulties achieving SCF convergence for the excitation energies using pure GGA or the asymptotically corrected functionals.

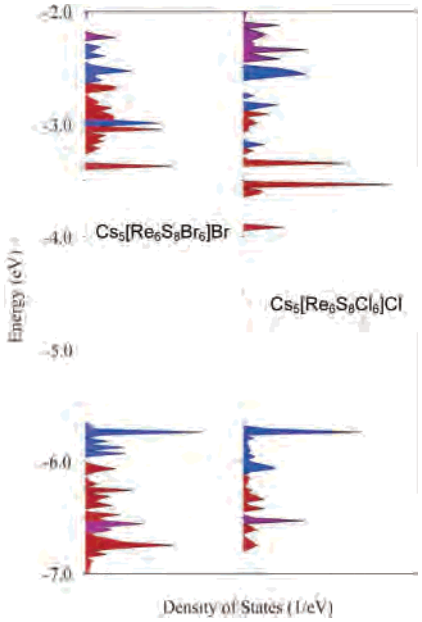

Figure 7. DOS and MO plots for $Cs_4[Re_6S_8X_6]\cdot CsX$ (X = Cl, Br). Blue peaks represent the band levels which are predominantly localized on **B** clusters (see Figure 5). Red peaks are predominately associated with the **A** clusters. The violet peaks correspond to orbitals spread over **A** and **B**.

Table 3. Mulliken Charge Analysis of $Cs_4[Re_6S_8X_6]\cdot CsX$ (X = Cl, Br) for the Center- and Corner-Residing Clusters within the Unit Cell

	center cluster	corner cluster
$Cs_4[Re_6S_8Cl_6]\cdot CsCl$	−2.654	−2.820
$Cs_4[Re_6S_8Br_6]\cdot CsBr$	−2.616	−2.716

the second $^1T_{1u} \leftarrow {}^1A_{1g}$ state. The triplet−singlet emission energies confirm previous calculations, and we predict that the orbital energy contribution to the emission is ∼98% LUMO to HOMO. The LB94 excitation energies are, on average, closer to experimental results but still overestimate the energies of the spin and orbitally forbidden transitions.

Solid-State Effects. There are fundamental uncertainties surrounding any computational attempt to model the electronic structure of molecules/ions for which spectroscopic measurements have been performed in solution with computations using molecules/ions in vacuo. When molecular ions bear substantial negative charges, it is reasonable to assume that the predominant uncertainties in the vacuum calculations are attributable to the missing electrostatic stabilization conferred by the (screened) counterions in the condensed phase. Solid-state calculations on comparatively "simple" salts of these anionic clusters, where the surrounding cations provide a realistic Madelung potential, provide useful information concerning the uncertainties—whether they are compared with measurements on more complex salts (with larger organic counterions) or with solution.

$Cs_4[Re_6S_8X_6]\cdot CsX$ (X = Cl, Br) crystallizes in the trigonal-hexagonal space group $R\bar{3}c$ with 2 (6) clusters per rhombohedral (trigonal-hexagonal) cell. [25,26] The crystal structure is shown in Figure 5. The Re_6 octahedra reside on a $\bar{3}$ (S_6) symmetry site, but possess near-D_{3d} symmetry. The Re−Re bond distances are nearly equal (2.594 and 2.603 Å), Re−S

(95) See the Supporting Information for a list of emission lifetimes.

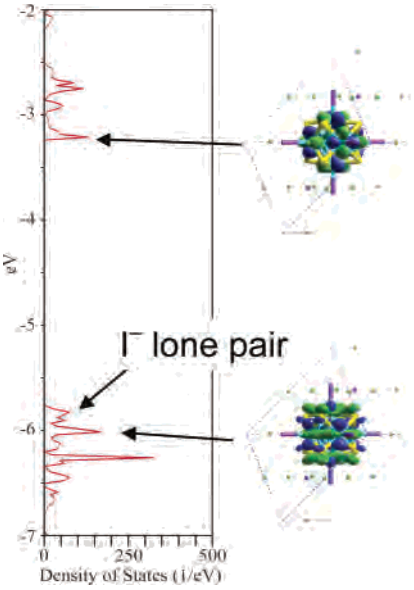

Figure 8. DOS in the frontier orbital range for $Cs_4[Re_6S_8I_6]\cdot 2CsI$.

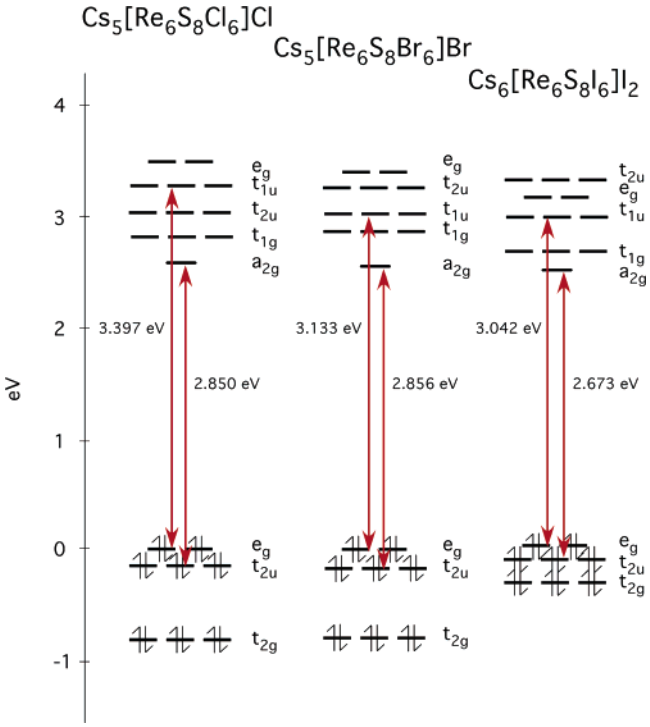

Figure 9. Cluster orbital energies ($\boldsymbol{k}$ = 0) for $Cs_4[Re_6S_8I_6]\cdot 2CsI$ and for the **B** cluster in $Cs_4[Re_6S_8X_6]\cdot CsX$ (X = Cl, Br).

bond distances involving the sulfur atom on the 3-fold axis are 2.199 Å, and the other Re−S distances are 2.398 Å. The halide bond lengths are equal. In our studies, the space group symmetry was lowered to $R\bar{3}$ by localizing a halide ion in one of two (half-occupied) symmetry-equivalent sites (in $R\bar{3}c$). Using the rhombohedral setting, eight cesium cations and two CsX units surround the two cluster units whose centers are located at (0,0,0) and ($^1/_2$,$^1/_2$,$^1/_2$).

$Cs_4[Re_6S_8I_6]\cdot 2CsI$ crystallizes in the cubic space group $Fm\bar{3}m$ with one (four) cluster(s) per primitive (conventional) cell (Figure 6).[25] The Re_6 octahedron resides on an $m\bar{3}m$ symmetry site and exhibits O_h symmetry. The Re−Re bond distances are 2.608 Å, Re−S bond distances are 2.408 Å,

Table 4. Comparison of the Single-Cluster vs Solid-State Orbital Energy Differences Based on the BLYP Functional

		ADF			$DMol^3$	
		gas phase			gas phase	solid state
	expt (eV)[25,28]	singlet−singlet excitation (eV)[a]	scalar orbital energy difference (eV)	spin−orbit orbital energy differences (eV)[b]	orbital energy difference (eV)	orbital energy difference (eV)
		$e_g \rightarrow t_{1u}$	$e_g \rightarrow t_{1u}$	$e_g \rightarrow t_{1u}$	$e_g \rightarrow t_{1u}$	$t_{2u} \rightarrow a_{2g}$
$Re_6S_8Cl_6^{4-}$	2.857	2.999	2.953	2.633	3.225	2.828
$Re_6S_8Br_6^{4-}$	2.798	2.815	2.766	2.447	2.781	2.775
$Re_6S_8I_6^{4-}$	2.445	2.553	2.501	2.209	2.515	2.672
		$t_{2u} \rightarrow a_{2g}$	$t_{2u} \rightarrow a_{2g}$	$t_{2u} \rightarrow a_{2g}$	$t_{2u} \rightarrow a_{2g}$	$e_g \rightarrow t_{1u}$
$Re_6S_8Cl_6^{4-}$	3.289	3.2833	3.259	2.930	3.153	3.397
$Re_6S_8Br_6^{4-}$	3.092	3.3080	3.285	2.939	3.221	3.133
$Re_6S_8I_6^{4-}$	2.952	3.2324	3.213	2.704	3.115	3.042
mean[c]		0.126	0.091	0.262	0.096	0.069
RMS		0.162	0.141	0.272	0.183	0.111
$e_g \leftarrow a_{2g}$[d]						
$Re_6S_8Cl_6^{4-}$	1.645	2.519	2.686	2.543	2.685	2.608
$Re_6S_8Br_6^{4-}$	1.5932	2.522	2.721	2.582	2.688	2.629
$Re_6S_8I_6^{4-}$	1.5450	2.441	2.687	2.478	2.615	2.593

[a] Orbital assignments are from the dominant excitation contribution. [b] See Supporting Information for complete information. [c] Mean is the calculated value minus experiment. [d] The $e_g \leftarrow a_{2g}$ emission comparison are not included in an error analysis of the data since the calculated data derived from O_h geometries and a proper treatment of the emission data takes into account the Jahn−Teller distortion; see Supporting Information and ref 36.

and Re−I distances are 2.779 Å. In our studies, we used the primitive setting with the unit cell containing one cluster unit surrounded by six cesium cations and two iodide anions.

Figure 7 shows the density of states (DOS) plot for the chloride and bromide complexes. In contrast to the situation for polyanionic clusters in a vacuum, the cluster bonding bands are stabilized because the clusters reside within a realistic solid-state Madelung potential (in our case, the cesium ions). The $R\bar{3}$ structure contains two distinct clusters (at 0,0,0 and $^1/_2,^1/_2,^1/_2$) with slightly different Madelung potentials that emerge from this calculation with slightly different charges (Table 3). Mulliken charge analysis shows that the cluster located at the center of the cell bears a greater negative charge than the cluster at the origin. In the "true" $R\bar{3}c$ space group, these two clusters are equivalent, so the different cluster potentials (and computed charges) may either be seen as an artifact of our $R\bar{3}$ structural choice or as more realistically reflective of the spread in potentials that clusters in a real crystal experience due to variations in occupation of the nearby disordered halide position (labeled X(1) and X(2) in Figure 5). There is an orbital energy-level shift between the two different clusters in the chloride (bromide) compound(s) of ∼0.7 eV (∼0.4 eV), so while a cursory glance at the DOS plot reveals that the solid has a band gap of ∼1.7 eV, the band gap for each individual cluster is ∼2.6 eV. Calculations at a single ***k***-point ($\boldsymbol{k} = 0$), show again that the HOMO is the e_g orbital, as in the gas-phase anion, and the LUMO remains the a_{2g} (Figure 7).

The DOS plot for $Cs_4[Re_6S_8I_6]\cdot 2CsI$ in Figure 8 reveals that the bands at the Fermi energy are mainly localized at the unbound iodide ion. Approximately 0.2 eV lower reside the cluster bonding orbitals. Calculations at a single ***k***-point ($\boldsymbol{k} = 0$) show again that the cluster HOMO is the e_g orbital and the LUMO remains the a_{2g} (Figure 8).

Since these solids contain discrete clusters, one can generate a molecular orbital diagram to describe the features of the DOS in each case. Figure 9 depicts the energy levels at $\boldsymbol{k} = 0$ for the cluster orbitals in $Cs_4[Re_6S_8I_6]\cdot 2CsI$ and for the center clusters in $Cs_4[Re_6S_8X_6]\cdot CsX$ (X = Cl, Br). Again, the relative orbital energies have been shifted so that the e_g (HOMOs) are at the same level. The diagrams show that upon moving from Cl to Br and I, there is a downward shift of Re−X antibonding orbitals (t_{1u} and e_g), as is seen in the case of the isolated clusters, but it is not as dramatic compared to the gas-phase calculations. The t_{2g} and t_{2u} orbitals are also affected and become (relatively) destabilized upon moving from Cl to I. The relative energies of the a_{2g}, t_{1g}, and t_{2u} antibonding orbitals remain virtually unchanged through the series. Table 4 shows the orbital energy differences of the e_g to t_{1u}, t_{2u} to a_{2g}, and e_g to a_{2g} set of orbitals. These orbital energy differences can serve as a first-order approximation to transition energies since TDDFT has not been implemented in $DMol^3$. Because the solid-state calculations were performed using $DMol^3$, the orbital energy differences for the single-cluster calculations are also given using $DMol^3$ in order to maintain the same functional and numerical basis in the vacuum and solid-state calculations. For further comparison, the single-cluster singlet−singlet excitation energy and orbital energy differences reported in the previous section using the ADF program are given alongside the $DMol^3$ data. All values reported in Table 4 use the experimental geometries and the BLYP functional.

Among the most significant differences between the vacuum and solid-state molecular orbital diagrams are seen in the relatively higher energies of the antibonding t_{1u} and e_g orbitals in the solid-state case (Figure 10). Interestingly, the orbital energy differences, $E(a_{2g}) - E(t_{2u})$ and $E(t_{1u}) - E(e_g)$, are inverted in the solid state; the difference between the cluster−ligand pπ-to-metal−metal antibonding orbitals is predicted to be smaller and comparable to the experimental first excitation energy. The latter orbital energy difference, $E(t_{1u}) - E(e_g)$, is closer to the second excitation energy. In contrast, the e_g (HOMO)-to-a_{2g} (LUMO) orbital energy differences for the solid state compound and single cluster are quite comparable; both overestimate the observed emission energy by the same margin. The presence of the charge

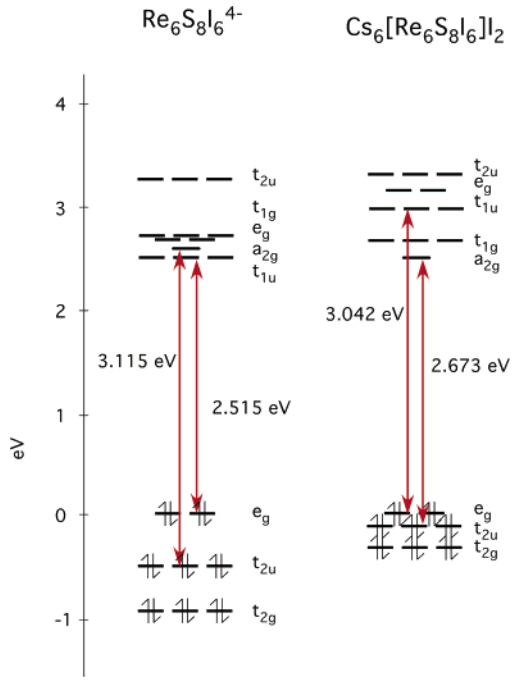

Figure 10. Vacuum and solid-state ($\boldsymbol{k} = 0$) molecular orbital diagrams using the BLYP functional from DMol^3 calculations.

compensation provided by the cesium ions in the solid apparently has a somewhat different effect on orbitals localized in different regions of the cluster. As we have seen, all the orbitals in the frontier orbital energy range shift upon moving from the vacuum to the solid by a similar amount; both the e_g (HOMO) and a_{2g} (LUMO) are built up almost entirely from the same rhenium 5d(δ) orbitals on the clusters, so their relative energies are almost exactly unchanged. The σ^* (t_{1u} and e_g) and π^* (t_{2u}) orbitals, on the other hand, have some significant terminal halide admixture, and the differential stabilization provided by the Madelung potentials has resulted in a relative upward shift of these orbitals. It seems likely that these characteristics would carry over to results obtained with other functionals, were those available.

Conclusions

The transition energies discussed here were not, of course, measured on clusters in a vacuum or ensconced within the solids used for our solid-state calculations. If trends in orbital energy differences are any guide, then the differences we see between solid-state and vacuum calculations indicate that *imprecision in calculated transition energies for highly charged species may be as much a problem associated with the use of isolated ions in calculations as with the use of any particular computational method*. We are inclined to believe that these solid-state calculations, in which a realistic condensed phase (and charge compensated) environment is used, provide a preferable approximation to a cluster's environment in solution than does a vacuum, in which no charge compensation is included.

Acknowledgment. We wish to thank Dr. Lisa Perez for valuable help and discussions. We thank the Robert A. Welch Foundation for its support through Grant No. A-1132 and the Texas Advanced Research Program through Grant No. 010366-0188-2001. We also thank the Supercomputing Facility at Texas A&M and the Laboratory for Molecular Simulation for computing time and other support.

Supporting Information Available: Calculated oscillator strengths of the $^1T_{1u} \leftarrow {}^1A_{1g}$ excitation for $[Re_6S_8X_6]^{4-}$ (X = Cl, Br, I), discussion of the geometry optimization calculations for $[Re_6S_8X_6]^{4-}$ (X = Cl, Br, I); experimental data of the luminescence lifetimes for $(Bu_4N)_4[Re_6S_8X_6]$ (X = Cl, Br, I) and $(Bu_4N)_2[M_6X_{14}]$ (M = Mo, W; X = Cl, Br); and discussion of spin−orbit calculations. This material is available free of charge via the Internet at http://pubs.acs.org.

IC061061M